A LETTERS JOURNAL EXPLORING THE FRONTIERS OF PHYSICS

Società Italiana di Fisica

edp sciences

IOP Institute of Physics

LETTER

Temperature-dependent transformation multiphysics and ambient-adaptive multiphysical metamaterials

To cite this article: M. Lei *et al* 2021 *EPL* **135** 54003

A Letters Journal Exploring the Frontiers of Physics

September 2021

EPL, **135** (2021) 54003
www.epljournal.org
doi: 10.1209/0295-5075/ac159d

Temperature-dependent transformation multiphysics and ambient-adaptive multiphysical metamaterials

M. Lei[1,2(a)], J. Wang[1,2,3(a)(b)], G. L. Dai[4], P. Tan[1(c)] and J. P. Huang[1,2(d)]

[1] *Department of Physics and State Key Laboratory of Surface Physics, Fudan University - Shanghai 200438, China*
[2] *Key Laboratory of Micro and Nano Photonic Structures (MOE), Fudan University - Shanghai 200438, China*
[3] *School of Physics, East China University of Science and Technology - Shanghai 200237, China*
[4] *School of Sciences, Nantong University - Nantong 226019, China*

received 16 April 2021; accepted in final form 19 July 2021
published online 8 November 2021

Abstract – Temperature-dependent transformation thermotics provides a powerful tool for designing multifunctional, switchable, or intelligent metamaterials in diffusion systems. However, its extension to multiphysics lacks study, in which temperature dependence of intrinsic parameters is ubiquitous. Here, we theoretically establish a temperature-dependent transformation method for controlling multiphysics. Taking thermoelectric transport as a representative case, we analytically prove the form invariance of its temperature-dependent governing equations and definitively formulate the corresponding transformation rules. Finite-element simulations demonstrate solid and robust thermoelectric cloaking, concentrating, and rotating performance in temperature-dependent backgrounds. Two practical applications are further designed with temperature-dependent transformation: one is an ambient-responsive cloak-concentrator thermoelectric device that can switch between cloaking and concentrating; the other is an improved thermoelectric cloak with nearly thermostat performance inside. Our theoretical frameworks and application design may provide guidance for efficiently controlling temperature-related multiphysics and enlighten subsequent intelligent multiphysical metamaterial research.

Introduction. – Recent advances in metamaterials and metadevices for controlling diffusion systems have witnessed a development tendency of adaptability, adjustability, and integration [1–5]. The nonlinear transformation thermotics [6–8], evolving from the linear transformation theory [9–13], provides a definite method to exactly map the diffusive single-field distribution to a required one in temperature-dependent backgrounds. On the basis of it, metamaterial research for manipulating diffusive flows achieves enhanced convertibility [14–17] and intellectualization [18–21].

However, in practical applications, it is important to consider how to manipulate multiphysics, which is ubiquitous in nature, industry, and daily life. Until now, almost all efforts in controlling multiphysics have been confined to linear media [22–30]. This approximation may not only deviate from practical situations to some extent, but also limit the advancement on manipulating multiple fields. Referring to thermoelectric (TE) effects [31–33], temperature-dependent transport processes have been investigated due to the electron-phonon coupling mechanism [34–36] or strong interaction in quantum-dot systems [37,38]. At the macroscopic level, nonlinearity of materials is often embodied in temperature-dependent thermal conductivities, electrical conductivities, and Seeback coefficients [39], which may introduce better TE performance beyond linear response to temperature or voltage bias [40]. In detail, the thermal conductivity κ may have a power-law form T^n (n is a real number) with different experiential values of n for different conditions or materials, which induce different electrical conductivities according to the Wiedemann-Franz law [41]. The Seeback coefficient S is usually directly proportional to T for metals and some semiconductors [42]. Although nonlinear transformation thermotics can extended to decoupled multiphysics readily due to the form similarity of independent governing equations, it needs to be further studied if the nonlinear transformation theory still works in regulating coupled multiphysical fields like thermoelectricity.

(a) These authors contributed equally to this work.
(b) E-mail: 18110190048@fudan.edu.cn (corresponding author)
(c) E-mail: tanpeng@fudan.edu.cn
(d) E-mail: jphuang@fudan.edu.cn

Inspired by the nonlinear transformation thermotics [6–8], we extend it to the temperature-dependent TE transport where material properties and/or spatial transformation operations are temperature dependent. In this way, functions of passive devices may become flexible and able to automatically adapt to changes in environments. Our study represents an example of how to apply the temperature-dependent transformation theory to design intelligent multiphysical metamaterials and metadevices, which can be generalized to other multiphysics.

Theory. – We consider a nonlinear TE coupling transport process as a representative temperature-dependent multiphysics case. First, the nonlinearity indicates the temperature dependence of electrical conductivity, which has been adequately studied. The general form of a temperature-dependent electrical conductivity tensor can be written as $\boldsymbol{\sigma}(T)$. On the other hand, according to the Wiedemann-Franz law [43], a considerable amount of materials with electron domination in heat conduction will thus have temperature-dependent thermal conductivity tensors $\boldsymbol{\kappa}(T)$. In addition, a nonlinear Seebeck coefficient tensor is given as $\boldsymbol{S}(T)$ without loss of generality. When the temperature and voltage biases are applied on the TE medium simultaneously, the coupled heat and electrical currents will be induced by each other separately besides their respective independent transport. Thus, the constitutive relations of electric current density $\boldsymbol{J}$ and heat current density $\boldsymbol{J}_Q$ can be described as [44,45]

$$\begin{aligned} \boldsymbol{J} &= -\boldsymbol{\sigma}(T)\boldsymbol{\nabla}\mu - \boldsymbol{\sigma}(T)\boldsymbol{S}(T)\boldsymbol{\nabla}T, \\ \boldsymbol{J}_Q &= -\boldsymbol{\kappa}(T)\boldsymbol{\nabla}T + T\boldsymbol{S}^{\mathrm{tr}}(T)\boldsymbol{J}, \end{aligned} \tag{1}$$

where μ and T are the position-related electrochemical potential and temperature, and $\boldsymbol{S}^{\mathrm{tr}}(T)$ is the transpose of $\boldsymbol{S}(T)$. Charge and heat flows are coupled by the Seebeck coefficient $\boldsymbol{S}(T)$. At the steady state with local equilibrium, the governing equations of TE transport are expressed as [44,45]

$$\begin{aligned} \boldsymbol{\nabla}\cdot\boldsymbol{J} &= 0, \\ \boldsymbol{\nabla}\cdot\boldsymbol{J}_Q &= -\boldsymbol{\nabla}\mu\cdot\boldsymbol{J}. \end{aligned} \tag{2}$$

In contrast with single physics, TE coupling transport leads to the generation of a heat source term, namely, $-\boldsymbol{\nabla}\mu\cdot\boldsymbol{J}$, which can be interpreted as a Joule heating result. With the Onsager reciprocal requirement [46], electrical and thermal conductivity tensors should be symmetric. Thus, we can determine that $\boldsymbol{\sigma}(T) = \boldsymbol{\sigma}^{\mathrm{tr}}(T)$ and $\boldsymbol{\kappa}(T) = \boldsymbol{\kappa}^{\mathrm{tr}}(T)$. Substituting eq. (1) into eq. (2), the governing equations can be rewritten, respectively, as

$$\boldsymbol{\nabla}\cdot[\boldsymbol{\sigma}(T)\boldsymbol{\nabla}\mu + \boldsymbol{\sigma}(T)\boldsymbol{S}(T)\boldsymbol{\nabla}T] = 0, \tag{3}$$

and

$$\begin{aligned} &-\boldsymbol{\nabla}\cdot[\boldsymbol{\kappa}(T)\boldsymbol{\nabla}T + T\boldsymbol{S}^{\mathrm{tr}}(T)\boldsymbol{\sigma}(T)\boldsymbol{S}(T)\boldsymbol{\nabla}T \\ &+ T\boldsymbol{S}^{\mathrm{tr}}(T)\boldsymbol{\sigma}(T)\boldsymbol{\nabla}\mu] = \\ &\boldsymbol{\nabla}\mu\cdot[\boldsymbol{\sigma}(T)\boldsymbol{\nabla}\mu + \boldsymbol{\sigma}(T)\boldsymbol{S}(T)\boldsymbol{\nabla}T]. \end{aligned} \tag{4}$$

We are now in the position to prove that eqs. (3) and (4) satisfy form invariance under arbitrary coordinate transformation, so that the transformation theory is still valid in the temperature-dependent TE transport process. In a curvilinear coordinate system with a set of contravariant bases $\{\boldsymbol{g}^i, \boldsymbol{g}^j, \boldsymbol{g}^k\}$, a group of covariant bases $\{\boldsymbol{g}_i, \boldsymbol{g}_j, \boldsymbol{g}_k\}$, and corresponding contravariant components (x^i, y^j, z^k), the component form of eq. (3) can be expressed as

$$\partial_i[\sqrt{g}\sigma^{ij}(T)\partial_j\mu] + \partial_i[\sqrt{g}\sigma^{ij}(T)S_j^k(T)\partial_k T] = 0, \tag{5}$$

where g is the determinant of the matrix with components $g_{ij} = \boldsymbol{g}_i\cdot\boldsymbol{g}_j$. And the component form of eq. (4) can be written as

$$\begin{aligned} &\partial_j[\sqrt{g}\kappa^{jk}(T)\partial_k T + T\sqrt{g}(S^{\mathrm{tr}})_i^j(T)\sigma^{ij}(T)S_j^k(T)\partial_k T \\ &+ T\sqrt{g}(S^{\mathrm{tr}})_i^j(T)\sigma^{ij}(T)\partial_j\mu] = \\ &-\sqrt{g}(\partial_j\mu)[\sigma^{ij}(T)\partial_j\mu + \sigma^{ij}(T)S_j^k(T)\partial_k T], \end{aligned} \tag{6}$$

where $(S^{\mathrm{tr}})_i^j(T)$ is the transpose of $S_i^j(T)$. Equations. (5) and (6) have the same form under different coordinates. The only difference in diverse coordinate systems is the coefficient g. Here, g is not limited to position dependence and can be written as $g(T)$ if the coordinate transformation is temperature dependent. The theory for temperature-dependent transformation TE fields allows executing temperature-dependent coordinate transformations on temperature-dependent TE materials, and these two kinds of nonlinearity will be incorporated into transformed physical parameters.

For the simplicity of derivation on transformation rules, we first demonstrate the linear transformation. Now, consider a bijection $f\colon \boldsymbol{r}\mapsto\boldsymbol{r}'$, which is smooth enough from the pretransformed space to the transformed space in the three-dimensional Euclidean space. Due to the diffeomorphism between the pretransformed space (virtual space) with a chosen set of curvilinear coordinates $\{x, y, z\}$ and the transformed space (physical space) with another set of Cartesian coordinates $\{x', y', z'\}$, eqs. (3) and (4) can be rewritten as

$$\boldsymbol{\nabla}'\cdot[\boldsymbol{\sigma}'(T')\boldsymbol{\nabla}'\mu' + \boldsymbol{\sigma}'(T')\boldsymbol{S}'(T')\boldsymbol{\nabla}T'] = 0, \tag{7}$$

and

$$\begin{aligned} &-\boldsymbol{\nabla}'\cdot[\boldsymbol{\kappa}'(T')\boldsymbol{\nabla}'T' + T'(\boldsymbol{S}')^{\mathrm{tr}}(T')\boldsymbol{\sigma}'(T')\boldsymbol{S}'(T')\boldsymbol{\nabla}'T' \\ &+ T'(\boldsymbol{S}')^{\mathrm{tr}}(T')\boldsymbol{\sigma}'(T')\boldsymbol{\nabla}'\mu'] = \\ &\boldsymbol{\nabla}'\mu'\cdot[\boldsymbol{\sigma}'(T')\boldsymbol{\nabla}'\mu' + \boldsymbol{\sigma}'(T)\boldsymbol{S}'(T')\boldsymbol{\nabla}'T']. \end{aligned} \tag{8}$$

We can find that transformation rules given by eqs. (3) and (4) are consistent with eq. (7) and eq. (8). The transformed $\boldsymbol{\kappa}'(T')$, $\boldsymbol{\sigma}'(T')$ and $\boldsymbol{S}'(T')$ can be expressed as

$$\boldsymbol{\kappa}'(T'(\boldsymbol{r}')) = \frac{\mathsf{A}\boldsymbol{\kappa}_0(T(f^{-1}(\boldsymbol{r}')))\mathsf{A}^{\mathrm{tr}}}{\det\mathsf{A}}, \tag{9}$$

$$\boldsymbol{\sigma}'(T'(\boldsymbol{r}')) = \frac{\mathsf{A}\boldsymbol{\sigma}_0(T(f^{-1}(\boldsymbol{r}')))\mathsf{A}^{\mathrm{tr}}}{\det\mathsf{A}}, \tag{10}$$

$$\boldsymbol{S}'(T'(\boldsymbol{r}')) = \mathsf{A}^{-\mathrm{tr}}\boldsymbol{S}(T(f^{-1}(\boldsymbol{r}')))\mathsf{A}^{\mathrm{tr}}. \tag{11}$$

The linear transformation on temperature-dependent TE background requires tailoring of thermal conductivity, electrical conductivity, and Seebeck coefficient described in eqs. (9)–(11).

Next, we return to the theory of nonlinear TE transformation, that is, to perform temperature-dependent transformation on temperature-dependent TE backgrounds. Temperature-dependent transformation means that the transformed operations are temperature related, so the corresponding Jacobian matrixes become $\mathsf{A}(T)$. We can see that the transformation rules of linear transformation can easily be generalized to the nonlinear transformation by replacing r' with $r'(T)$ and replacing A with $\mathsf{A}(T)$ in eqs. (9), (10), and (11).

Simulation. – We now employ these rules to design TE metamaterials on temperature-dependent backgrounds. Equation (10) implies that the Seebeck coefficient remains invariant after coordinate transformation if the Seebeck coefficient before transformation is isotropic, it can be written as $S'(T) = S_0(T) = \gamma T$ (γ is constant). The temperature-dependent electrical conductivity and thermal conductivity satisfy the transformation rules in eqs. (9) and (11). Here, we assign the background thermal conductivity a trivial scalar expression $\kappa_0(T) = \alpha + \beta T^n$ (α, β and n are constants). According to the Wiedemann-Franz law $\kappa/\sigma = LT$ (L is the Lorenz number) [43], the background electrical conductivity can be written as $\sigma_0(T) = (\alpha T^{-1} + \beta T^{n-1})/L$. The transformed material properties can then be expressed as

$$\begin{aligned} \boldsymbol{\kappa}'(T) &= \frac{\mathsf{A}(\alpha+\beta T^n)\mathsf{A}^{\mathrm{tr}}}{\det \mathsf{A}}, \\ \boldsymbol{\sigma}'(T) &= \frac{\mathsf{A}(\alpha+\beta T^n/(LT))\mathsf{A}^{\mathrm{tr}}}{\det \mathsf{A}}, \\ S'(T) &= \gamma T. \end{aligned} \tag{12}$$

Here, we consider functionalities of cloaking, concentrating and rotating in two-dimensional nonlinear backgrounds. The TE cloak keeps the central region free from heat flows and currents to maintain constant temperatures and electric potentials without disturbing TE distributions outside, as shown in fig. 1(a). We can present the coordinate transformation relationship of the cloak in polar coordinates (r,θ) as

$$r' = r(r_2 - r_1)/r_2 + r_1, \quad \theta' = \theta, \tag{13}$$

where $r \in [0, r_2]$ and $r' \in [r_1, r_2]$. The purpose of a TE concentrator is to collect more currents and heat flows in the central region to increase the local temperature gradient without disturbing the TE distribution outside, as shown in fig. 1(b). The detailed coordinate transformation can be given as

$$\begin{aligned} &r'' = r_1 r/r_m \quad (r < r_m), \\ &r'' = r(r_2 - r_1)/(r_2 - r_m) \\ &\qquad + r_2(r_1 - r_m)/(r_2 - r_m) \quad (r_m < r < r_2), \\ &\theta'' = \theta, \end{aligned} \tag{14}$$

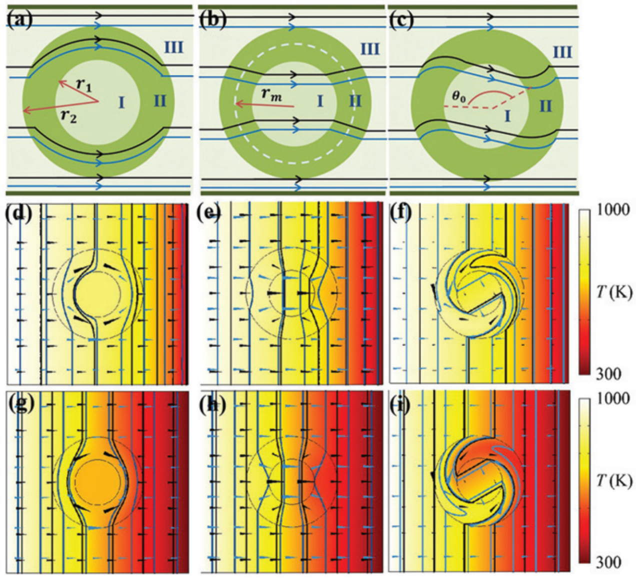

Fig. 1: (a)–(c) Schematic graphs of a TE cloak, concentrator, and rotator located in the center of a temperature-dependent background. Region I, II and III represent the functional area, transformation layer, and background, respectively. Panels (d)–(f) and (g)–(i) are simulation results of temperature-dependent and temperature-independent TE cloak, concentrator and rotator, separately. Background size is 8×8 cm. The inner radius of the transformed layer is $r_1 = 1$ cm and the outer radius is $r_2 = 2$ cm. The virtual radius of concentrator is $r_m = 1.5$ cm, and the rotation angle of rotator is $\theta_0 = 120°$. The background thermal conductivity of (d)–(f) is $100 + 10T^3$ W/(m · K), the electrical conductivity is $100/T + 10T^2$ S/m, and the Seebeck coefficient is $S = 30T\,\mu$V/K. The background thermal conductivity of (g)–(i) is 1000 W/(m · K), the electrical conductivity is 100 S/m, and the Seebeck coefficient is $S = 200\,\mu$V/K. The left boundary is set as 1000 K and 0.01 V, and the right boundary is set as 300 K and 0 V. Upper and lower boundaries are thermally and electrically insulated. In (d)–(i), color surfaces represent temperature distribution, black and blue arrows/lines denote thermal and electric flows/isothermal and isopotential.

where r_m is the radius between r_1 and r_2. A TE rotator serves to rotate the currents and heat flows with angle θ_0 in the central circular region without disturbing the TE distributions outside, as indicated in fig. 1(c). The corresponding coordinate transformation can be described as

$$\begin{aligned} &r''' = r, \\ &\theta''' = \theta + \theta_0 \quad (r < r_1), \\ &\theta''' = \theta + \theta_0(r - r_2)/(r_1 - r_2) \quad (r_1 < r < r_2). \end{aligned} \tag{15}$$

The Jacobian transformation matrix A can be expressed in polar coordinates as

$$\mathsf{A} = \begin{bmatrix} \partial r^*/\partial r & \partial r^*/(r\partial\theta) \\ r^*\partial\theta^*/\partial r & r^*\partial\theta^*/(r\partial\theta) \end{bmatrix}, \tag{16}$$

where $r^* = r', r''$ or r''' and $\theta^* = \theta', \theta''$ or θ'''. Substituting eqs. (13)–(15) into eq. (16), we can obtain the corresponding Jacobian matrices of three metamaterials. In combination with eq. (12), the transformed thermal conductivity and electrical conductivity of three metamaterials in the annulus region ($r_1 < r' < r_2$) can be expressed as

$$\begin{aligned}\boldsymbol{\kappa}'(T) &= (\alpha + \beta T^n)\ \mathrm{B}^*,\\ \boldsymbol{\sigma}'(T) &= (\alpha + \beta T^n)/(LT)\ \mathrm{B}^*,\end{aligned} \tag{17}$$

where $\mathrm{B}^* = \mathrm{B}'$, B'', and B''' corresponding to TE cloaks, concentrators and rotators. They can be written separately

$$\begin{aligned}\mathrm{B}' =&\ \mathrm{diag}[(\mathrm{r}'-\mathrm{r}_1)/\mathrm{r}', \mathrm{r}'/(\mathrm{r}'-\mathrm{r}_1)],\\ \mathrm{B}'' =&\ \mathrm{diag}\left[\frac{(\mathrm{r}_2-\mathrm{r}_\mathrm{m})\mathrm{r}'' - (\mathrm{r}_1-\mathrm{r}_\mathrm{m})\mathrm{r}_2}{(\mathrm{r}_2-\mathrm{r}_\mathrm{m})\mathrm{r}''},\right.\\ &\left.\frac{(r_2-r_m)r''}{(r_2-r_m)r''-(r_1-r_m)r_2}\right],\\ \mathrm{B}''' =&\left(\left[1, \frac{\theta_0 \mathrm{r}'''}{\mathrm{r}_1-\mathrm{r}_2}\right],\right.\\ &\left.\left[\frac{\theta_0 r'''}{r_1-r_2}, \left(\frac{\theta_0 r'''}{r_1-r_2}\right)^2+1\right]\right).\end{aligned} \tag{18}$$

For TE cloaks, concentrators and rotators, the electrical conductivities and thermal conductivities in the center circular region with radius r_1 are the same as the backgrounds, and they can be written as

$$\begin{aligned}\boldsymbol{\kappa}^*(T) &= (\alpha + \beta T^n)\ \mathrm{diag}[1,1],\\ \boldsymbol{\sigma}^*(T) &= (\alpha + \beta T^n)/(LT)\ \mathrm{diag}[1,1].\end{aligned} \tag{19}$$

We then execute finite-element simulations of the designed temperature-dependent and temperature-independent TE cloak, concentrator and rotator with the commercial software COMSOL Multiphysics [47]. We use the steady TE-effect module in the two-dimensional system to simulate the temperature and potential distributions of coupled TE fields; the results are shown in the second and third panels of fig. 1, respectively. In figs. 1(d)–(i), temperature or potential distributions in backgrounds are inhomogeneousunder horizontal external thermal and electrical fields due to the temperature-dependent parameters, but the cloaking, concentrating, or rotating functionalities are still valid. For further verifying the robustness of the proposed metamaterials, we subject them to different temperature boundary conditions; see fig. 2. We retain the electrical boundary conditions and fix the right boundary at 300 K. With increasing temperatures up to 1500 K at the left boundary, the nonlinearity effect gradually emerges, which can be seen from the isothermal lines. However, cloaking, concentrating, and rotating still function effectively. For clarity, the references with pure backgrounds are also displayed for comparison. Furthermore, we plot the simulation data of the central lines horizontally crossing the center of metamaterials in fig. 3. The results are echoed well in region III (outside metamaterials), indicating no distortion in backgrounds. It is noted

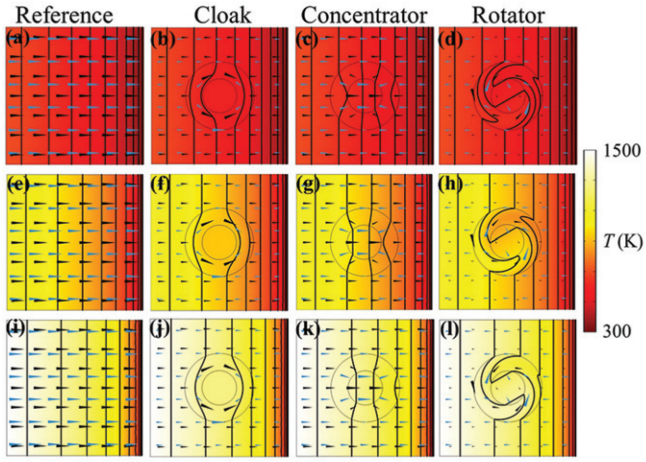

Fig. 2: Simulation results of the temperature-dependent TE cloak, concentrator, and rotator under different temperature boundary conditions. The parameter settings are the same as those in fig. 1. The right boundaries are set at 300 K thermally, with electrical grounding. The left boundaries are separately set at 700 K (a)–(d), 1100 K (e)–(h), 1500 K (i)–(l), and 0.01 V. Black and blue arrows indicate magnitudes and directions of heat and electric flows, respectively. References in the first column are bare backgrounds without any internal structures.

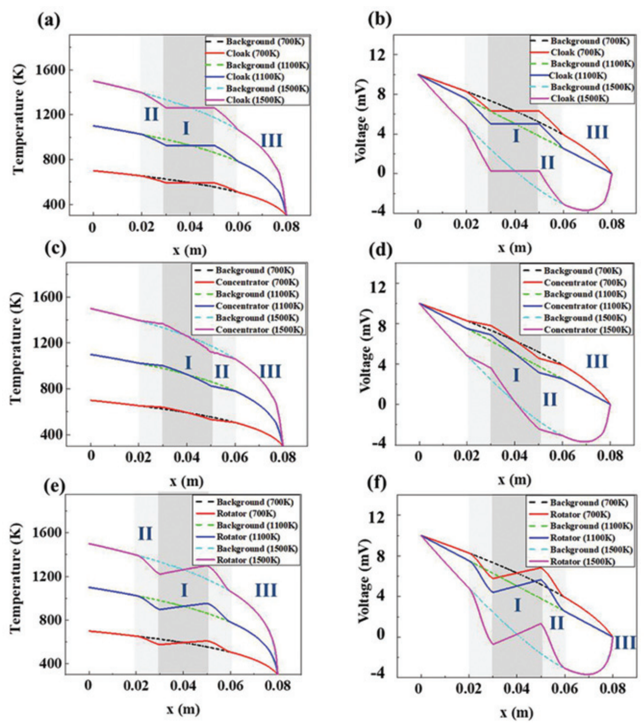

Fig. 3: Quantitative comparison between backgrounds assembled with metamaterials and bare backgrounds. The data are extracted at center lines along the horizontal direction from the simulation results in fig. 2. Three panels denote the cloak, concentrator, and rotator separately by row. The left and right columns are temperature and voltage data, respectively. Regions I, II, and III are the corresponding regions in fig. 1.

that relations between temperatures (or pontentials) and positions in region III are not linear but tend to nonlinearity with increasing high-temperature boundary conditions. In particular, voltages at 0.06–0.08 m show negative differentials, which is due to the coupled TE effects.

Application. –

A) Ambient-responsive TE cloak concentrator. Based on the proposed temperature-dependent transformation TE field theory, we further design an ambient-responsive TE cloak-concentrator device as a practical application. Due to the temperature-dependent features, cloaking and concentrating functionalities function under different environmental temperature regions, resulting in a switchable TE cloak concentrator. Here, we skip the original constitutive parameters and only consider the parameters after transformation operation. The emphasis of achieving TE cloak concentrator is to make the transformed thermal conductivity and electrical conductivity correspond to different functions under different temperatures. Thus we consider the temperature-related coordinate transformation to realize it. If we carefully check the coordinate transformation relationship in eqs. (13) and (14), we can find that eq. (14) has the same form as eq. (13) when $r_m = 0$. Thus, a temperature-dependent function can be constructed by replacing r_m in eq. (14) with $r_m^*(T)$, for which the coordinate transformation relationship corresponds to cloak at $r_m^*(T) = 0$ and concentrator at $r_m^*(T) = r_m$. Equation (13) can be rewritten as

$$r_m^*(T) = \frac{r_m}{1 + \exp[\eta(T - T_C)]}. \tag{20}$$

Here, T_C is a critical temperature around which $r_m^*(T)$ can be distinguished by 0 or r_m, as schematically shown in fig. 4(a). η is a scaling coefficient for ensuring the step change around T_C. The coordinate transformation of the shell region can be rewritten as

$$r' = r\frac{r_2 - r_1}{r_2 - r_m^*(T)} + r_2\frac{r_1 - r_m^*(T)}{r_2 - r_m^*(T)}, \quad \theta' = \theta, \tag{21}$$

where the transformed coordinates are temperature dependent, which also meets the requirements of nonlinear transformations. The expressions of transformed thermal and electrical conductivities can be obtained by replacing r_m in eq. (18) with $r_m^*(T)$, so expressions can be transformed into TE cloaks when the environment temperature is higher than T_C and into TE concentrators when the environment temperature is lower than T_C.

We present our results more intuitively by finite-element simulation. The simulation results are shown in figs. 4(b) and (c), according with the expected effects. The device shows concentrating within the temperature region of 300–320 K and cloaking from 340–360 K. That is, it can automatically transfer the function from TE cloaking (or concentrating) to TE concentrating (or cloaking) when the temperature of the environment changes. This is the direct result of ambient-responsive TE parameters and is impossible in linear transport processes. Additionally, we extract the data of temperature and voltage on the central line horizontally crossing the center in different temperature regions in figs. 4(d) and (e). Bakground temperature and potential data in region III coincide between with- and without-device cases, indicating that the background is not influenced. Cloaking and concentrating features are obvious in region I when comparing the slope with pure backgrounds.

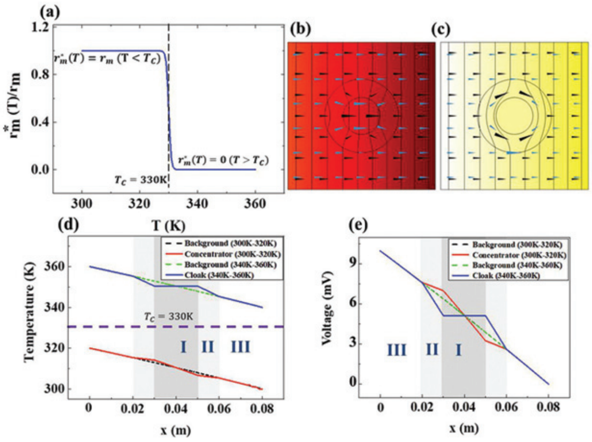

Fig. 4: TE cloak concentrator with different functions under different temperature regions. (a) The curve of $r_m^*(T)/r_m$ with temperature, and $T_C = 300\,\mathrm{K}$, $\eta = 2.5\,\mathrm{K}^{-1}$ in this expression of eq. (20). (b), (c): simulation results of the TE cloak concentrator. It exhibits concentration under the temperature region 300–320 K and cloaking under the temperature region 340–360 K. The higher temperature and voltage 0.01 V are set at the left boundaries, and the lower temperature and electrical grounding are set at the right boundaries. Panels (d) and (e) are the temperature and voltage curves of the center lines extracted from simulation results in (b) and (c). Regions I, II, and III are the corresponding regions in fig. 1.

Thermal conductivity and electrical conductivity of TE cloak concentrator are anisotropic and can achieve abrupt change in different temperature ranges. It is difficult for actual natural materials to meet this requirement. Shape memory alloys may be a candidate to achieve the switch of function [6,15] due to their sharp deformation with changing temperatures. Thus, we can employ composites of shape memory alloy and TE materials on the transformation layer to realize the ambient-responsive TE cloak concentrator.

B) Improved TE cloak. An improved TE cloak that can maintain a nearly constant temperature internally is designed. This is different from the existing TE cloak [29], in which the temperature inside relies on the boundary conditions. Four individual components compose the cloak, which is placed in a temperature-dependent background depicted as region III, as shown in fig. 5(a). A linear transformation is executed to region II, where the fixed thermal and electrical conductivities follow eq. (17). In

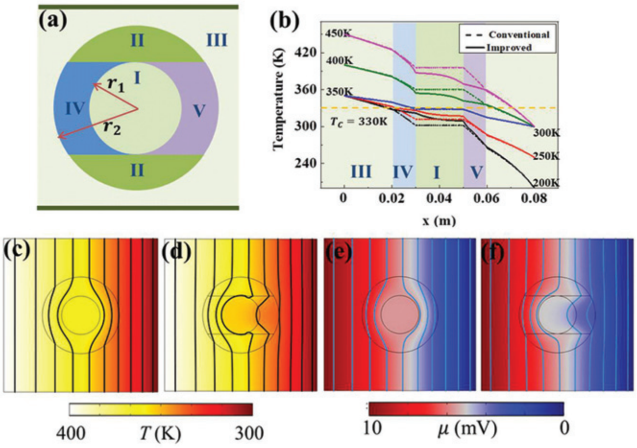

Fig. 5: Improved thermoelectric cloak. (a) Constituent structure. Panels (c) and (e) show the temperature and potential distributions of a conventional TE cloak, respectively. Panels (d) and (f) show the temperature and potential distributions of the improved TE cloak with near-thermostat functionality inside. The temperature 400 K and voltage 0.01 V are set at the left boundaries, and the temperature 300 K and electrical grounding are set at the right boundaries. Panel (b) denotes temperature curves of the center lines extracted from conventional cloak and improved cloaks. Different colors indicate different temperature conditions.

regions IV and V, the nonlinear transformation is achieved by two symmetrical equations: eq. (20) and

$$r_m^*(T) = \frac{r_m \exp[\eta(T - T_C)]}{1 + \exp[\eta(T - T_C)]}. \tag{22}$$

It is clear that eqs. (20) and (22) exhibit opposite behaviors around T_C. We obtain expressions of transformed thermal and electrical conductivities by substituting them into eq. (19). This operation may make the internal temperature approach T_C [15,16]. The temperature and voltage distributions of this cloak are shown in figs. 5(d) and (f). Clearly, we obtain simultaneous near-thermostat performance inside the cloak, while the distributions of temperature and potential remain unchanged outside the cloak. For comparison, we also demonstrate the conventional TE cloaks under the same boundary conditions in figs. 5(c) and (e). Furthermore, for quantitative verification, we extract temperature data of center lines from simulation results; see fig. 5(b). In region I, the temperature tends to T_C, which is marked as a yellow dashed line. Under changed high or low boundary temperatures, the designed cloak exhibits robustness in that the internal temperatures deviate to T_C, compared with conventional cloaks indicated by solid lines in fig. 5(b). In addition, in region III, good fitting of conventional and improved cloaks is visually concluded. Thus, the designed cloak can improve the thermostat performance internally without loss of concealing functionalities.

Discussion and conclusion. – We have verified that the form invariance of temperature-dependent TE governing equations remains valid under spatial coordinate transformation. It is noted that the temperature-dependent transformation emphasizes the transformation operation and backgrounds can depend on temperature simultaneously, usually leading to temperature-dependent design parameters. Recent studies in pyroelectricity [39–42] have shown that temperature dependence of TE materials is ubiquitous, especially on small scales, due to the corresponding large bias of temperature or voltage. From this perspective, the proposed temperature-dependent transformation multiphysics has general applicability for controlling TE fields with naturally existing materials.

As two representative applications of temperature-dependent TE transformation theory, ambient-responsive TE cloak-concentrator devices and improved TE cloaks are constructed by executing nonlinear transformation operation in nonlinear backgrounds. For the former, switching between cloaking and concentrating can be achieved under different ambient temperature regions. The devices can avoid thermal or electrical damage caused by high ambient temperatures, and heat and electric flows can be used effectively under low temperatures. For the latter, the desired temperature T_C can be approximately achieved inside the cloak. It is noted that the thermostat effects of improved TE cloaks are not strict due to the intrinsic limits of the transformed layers. That is, the zero thermal or electrical conductivities can be reached only at r_1, which limits physical spaces with respect to capturing specific temperatures [15,16]. However, the simulation results still show obvious improvement in internal temperature preservation *vs.* conventional cloaks. Although another solid scheme may resort to the bilayer design [15,16], here we verify that the transformed layers may also play the role of temperature trapper, which may be of benefit in some situations where the transformation method is employed.

In summary, the transformation theory on the nonlinear multiphysical backgrounds is established, so linear and nonlinear transformations can be performed on the background. Three nonlinear metamaterials with functions of cloaking, concentrating, and rotating are demonstrated, confirming the theory. As practical applications, two temperature-responsive multiphysical devices are designed, whose functionalities exceed those of their linear analogies. Our theory and design can be extended from thermoelectricity to other fields of multiphysics such as thermo-optics or thermomagnetics. For example, enhancement of magnetic field on a metal-coated superconductor thermomagnetic system will generate Joule heating sources [48]. The governing equation of the thermomagnetic effect in the superconductor satisfies the form invariance under coordinate transformation. Thus, the transformation theory can be used to control such thermomagnetic field. Various multiphysical intelligent metamaterials can be expected, which may not only facilitate multiple flow guidance but also be beneficial to the development of self-adaptation in metamaterial design.

* * *

We thank Prof. Kezhao Xiong and Mr. Fubao Yang for beneficial discussion. We acknowledge financial support from the National Natural Science Foundation of China under Grants No. 11725521 and No. 12035004, and from the Science and Technology Commission of Shanghai Municipality under Grant No. 20JC1414700.

Data availability statement: All data that support the findings of this study are included within the article (and any supplementary files).

REFERENCES

[1] Li Y., Li W., Han T., Zheng X., Li J., Li B., Fan S. H. and Qiu C.-W., *Nat. Rev. Mater.*, **6** (2021) 488.
[2] Yang S., Wang J., Dai G. L., Yang F. B. and Huang J. P., *Phys. Rep.*, **908** (2021) 1.
[3] Sklan S. R. and Li B. W., *Natl. Sci. Rev.*, **5** (2018) 138.
[4] Wang J., Dai G. L. and Huang J. P., *iScience*, **23** (2020) 101637.
[5] Dai G. L., *Front. Phys.*, **16** (2021) 53301.
[6] Li Y., Shen X. Y., Wu Z. H., Huang J. Y., Chen Y. X., Ni Y. S. and Huang J. P., *Phys. Rev. Lett.*, **115** (2015) 195503.
[7] Li Y., Shen X. Y., Huang J. P. and Ni Y. S., *Phys. Lett. A*, **380** (2016) 1641.
[8] Sklan S. R. and Li B. W., *Sci. Rep.*, **8** (2018) 4436.
[9] Fan C. Z., Gan Y. and Huang J. P., *Appl. Phys. Lett.*, **92** (2008) 251907.
[10] Chen T. Y, Weng C.-N. and Chen J.-S., *Appl. Phys. Lett.*, **93** (2008) 114103.
[11] Guenneau S., Amra C. and Veynante D., *Opt. Express*, **20** (2012) 8207.
[12] Narayana S. and Sato Y., *Phys. Rev. Lett.*, **108** (2012) 214303.
[13] Schittny R., Kadic M., Guenneau S. and Wegener M., *Phys. Rev. Lett.*, **110** (2013) 195901.
[14] Shen X. Y., Li Y., Jiang C. R., Ni Y. S. and Huang J. P., *Appl. Phys. Lett.*, **106** (2016) 031907.
[15] Shen X. Y., Li Y., Jiang C. R. and Huang J. P., *Phys. Rev. Lett.*, **117** (2016) 055501.
[16] Wang J., Shang J. and Huang J. P., *Phys. Rev. Appl.*, **11** (2019) 024053.
[17] Su C., Xu L. J. and Huang J. P., *EPL*, **130** (2020) 34001.
[18] Wehmeyer G., Yabuki T., Monachon C., Wu J. Q. and Dames C., *Appl. Phys. Rev.*, **4** (2017) 041304.
[19] Li Y., Li J. X., Qi M. H., Qiu C.-W. and Chen H. S., *Phys. Rev. B*, **103** (2021) 014307.
[20] Wang J., Dai G. L., Yang F. B. and Huang J. P., *Phys. Rev. E*, **101** (2020) 022119.
[21] Xu L. J., Huang J. P., Jiang T., Zhang L. and Huang J. P., *EPL*, **132** (2020) 14002.
[22] Li J. Y., Gao Y. and Huang J. P., *J. Appl. Phys.*, **108** (2010) 074504.
[23] Moccia M., Castaldi G., Savo S., Sato Y. and Galdi V., *Phys. Rev. X*, **5** (2014) 021025.
[24] Ma Y., Liu Y., Raza M., Wang Y. and He S., *Phys. Rev. Lett.*, **113** (2014) 205501.
[25] Raza M., Liu Y. and Ma Y., *J. Appl. Phys.*, **117** (2015) 024502.
[26] Lan C., Bi K., Fu X., Li B. and Zhou J., *Opt. Express*, **24** (2016) 23072.
[27] Lan C., Bi K., Fu X., Gao Z., Li B. and Zhou J., *Appl. Phys. Lett.*, **109** (2016) 201903.
[28] Fujii G. and Akimoto Y., *Appl. Phys. Lett.*, **115** (2019) 174101.
[29] Stedman T. and Woods L. M., *Sci. Rep.*, **7** (2017) 6988.
[30] Shi W. C., Stedman T. and Woods L. M., *J. Phys. Energy*, **1** (2019) 025002.
[31] He J. and Tritt T. M., *Science*, **357** (2017) 9997.
[32] Zhou X., Yan Y., Lu X., Zhu H., Han X., Chen G. and Ren Z., *Mater. Today*, **21** (2018) 974.
[33] Zevalkink A., Smiadak D. M., Blackburn J. L., Ferguson A. J., Chabinyc M. L. *et al.*, *Appl. Phys. Rev.*, **5** (2018) 021303.
[34] Melnick C. and Kaviany M., *Appl. Phys. Rev.*, **6** (2019) 021305.
[35] Karki D. B. and Kiselev M. N., *Phys. Rev. B*, **100** (2019) 125426.
[36] Zebarjadi M., Esfarjani K. and Shakouri A., *Appl. Phys. Lett.*, **91** (2007) 122104.
[37] Mazal Y., Meir Y. and Dubi Y., *Phys. Rev. B*, **99** (2019) 075433.
[38] Lavagna M., Talbo V., Duong T. Q. and Crepieux A., *Phys. Rev. B*, **102** (2020) 125426.
[39] Ishida A., *J. Appl. Phys.*, **128** (2020) 135105.
[40] Pourkiaei S. M., Hossein Ahmadi M., Sadeghzadeh M., Moosavi S., Pourfayaz F., Chen L. G., Yazdi M. A. P. and Kumar R., *Energy*, **186** (2019) 115849.
[41] Ziabari A., Zebarjadi M., Vashaee D. and Shakouri A., *Rep. Prog. Phys.*, **79** (2016) 095901.
[42] Snyder G. J. and Toberer E. S., *Nat. Mater.*, **7** (2008) 105.
[43] Tian Z., Lee S. and Chen G., *J. Heat Transf.*, **135** (2013) 061605.
[44] Tritt T. M. and Subramanian M. A., *Mater. Res. Soc. Bull.*, **31** (2006) 188.
[45] Domenicali C. A., *Rev. Mod. Phys.*, **26** (1954) 237.
[46] Onsager L., *Phys. Rev.*, **37** (1931) 405.
[47] `http://www.comsol.com/`.
[48] Vestgården J. I., Johansen T. H. and Galperin Y. M., *Low Temp. Phys.*, **44** (2018) 460.